DOI: 10.13009/EUCASS2022-6114
9TH EUROPEAN CONFERENCE FOR AERONAUTICS AND SPACE SCIENCES (EUCASS)

Development of CMC Combustion Chambers for Advanced Propellants in Space Propulsion

HEIDENREICH, Bernhard [1], WERLING, Lukas** [2], KURILOV Maxim[2], KIRCHBERGER; Christoph, DAUTH, Lucas[1], LEHNERT, Tobias, ELSÄßER, Henning[1], SELZER, Markus[1], SEILER, Helge[1]*

DLR – German Aerospace Center
[1] Institute of Structures and Design, Pfaffenwaldring 38-40, 70569 Stuttgart, Germany
[2] Institute of Space Propulsion, Lampoldshausen, Langer Grund, 74239 Hardthausen, Germany

Corresponding Author: Bernhard.Heidenreich@dlr.de
Email addresses: lukas.werling@dlr.de; Maxim.Kurilov@dlr.de; Cristoph.Kirchberger@dlr.de; Lucas.Dauth@dlr.de; Tobias.Lehnert@dlr.de; Henning.Elsaesser@dlr.de; Markus.Selzer @dlr.de; Helge.Seiler@dlr.de;

First Author and Second Author***
** DLR – German Aerospace Center, Institute of Structures and Design, Pfaffenwaldring 38-40, 70569 Stuttgart, Germany*
*** DLR – German Aerospace Center, Institute of Space Propulsion, Lampoldshausen, Langer Grund, 74239 Hardthausen, Germany*

Abstract

In the DLR project "Future Fuels", combustion chamber structures made of lightweight and high temperature stable ceramic matrix composites were in the focus of the development. In a first step, C/C-SiC tubes manufactured via the liquid silicon infiltration process and based on three different carbon fibre types and two different production methods for the CFRP preforms, were characterized. In biaxial pressure tests, all the different tubes could withstand the required inner pressure of 60 bar. Highest fracture strength was obtained with wet filament wound tubes based on ultra-high-modulus fibres, whereas tubes manufactured via prepreg wrapping using high tenacity fibre fabrics, offered a cost-effective alternative.

1. Introduction

Especially in tactical systems, where safety considerations play a crucial role, gelling oxidizers, fuels or monopropellants offer numerous advantages over using liquid propellants. For instance, in the case of a leak or a spill caused by loose pipework or perforations, a large liquid surface is not formed, and thus the danger of a large surface area fire is significantly lowered [1]. Additionally, gelation may also allow for a longer time to neutralize a spill, before propellant vapor concentration reaches dangerous levels. This is especially significant, if the spill occurs inside cramped spaces in ship magazines [2]. Additionally, since gels have a distinct yield point during storage, and are not liquified until pumped, they may hold particulate additives, which may be used to maximize energy density, or to render the propellants hypergolic [3]-[6].

However, there are also significant disadvantages to altering the rheology. If pumped through lines, gelled liquids have altered flow profiles (plug-flow, see [7] for further details), which may lead to higher pressure drops than in usual (i.e. Newtonian) liquids [8]. This may be a significant obstacle to the use of gelled propellant as regenerative coolant. To overcome this issue, also to dispose of the weight and complexity, added by implementing such a system, new iterations of ceramic matrix composite (CMC) materials are explored at DLR.

Since the late 1980´s, C/C-SiC materials have been developed at DLR [9], originally for the use in thermal protection systems for re-entry space vehicles. These materials are manufactured via a robust and relatively fast manufacturing

Copyright © 2022 by First Author and Second Author. Published by the EUCASS association with permission.

DOI: 10.13009/EUCASS2022-6114

method, the so-called liquid silicon infiltration (LSI). The LSI process can be subdivided in three main process steps. In the first process step, a CFRP (carbon fibre reinforced polymer) preform is manufactured by well-known manufacturing methods like autoclave technique, warm pressing, filament winding or resin injection, using commercially available carbon fibres and polymer precursors with high carbon yield, for example phenolic resins. In the second process step, the CFRP parts are pyrolyzed at a maximum temperature of 1650 °C in inert atmosphere, leading to carbon fibre reinforced carbon (C/C) preforms. In the third and last process step, the C/C preforms are siliconized at 1650 °C in vacuum. Thereby, molten Si is infiltrated in the porous C/C by capillary forces and the SiC matrix is built up by a chemical reaction of Si and C, leading to a final C/C-SiC material, characterized by dense bundles of carbon fibre reinforced carbon (C/C) embedded in a silicon carbide (SiC) matrix.

Due to the relatively fast process and the use of low-cost raw materials, LSI based CMC materials offer economic advantages compared to other CMC manufacturing methods like chemical vapor deposition (CVI) or polymer infiltration and pyrolysis (PIP). Therefore, LSI based CMC´s are the materials of choice for economically viable serial products like brake discs for automobiles [10], brake pads for high performance elevators [11] as well as for the propeller brake of the aircraft Airbus A 400 M [12].

Due to the unique combination of high temperature and thermal shock resistance with a low density (1.9 g/cm³), lightweight jet vanes for rocket motors could be developed successfully and transferred to industrial application [13]. During the last years, new C/C-SiC material variants based on high performance ultra-high-modulus (UHM) carbon fibres have been developed, [14] which offer increased mechanical strength and elastic modulus, compared to common materials based on high tenacity carbon fibres. Thereby, also the material composition changed, leading to an increased SiC phase content, without losing its quasiductile fracture behaviour. Due to the high SiC content, these materials generally show a higher abrasive and oxidation resistance, compared to carbon rich C/C-SiC standard materials, and therefore offer a high potential for the use in mechanically and thermally extremely loaded combustion chambers.

2. Sample Manufacture

In a first development step, CFRP tubes (Ø41/Ø 36, l = 500 mm) based on high tenacity fibres (HT, Tenax HTA 40) as well as on high performance intermodulus (IM, Torayca T800H) and ultra-high-modulus (UHM, NGF YS-90A) fibres were manufactured and characterized (Table 1).

Table 1 Overview of carbon fibres used for tube manufacture (manufacturers' data).

Fibre type		HT	IM	UHM
Fibre		HTA 40 E13 6K	T800H 12K	Granoc YS-90A-30S 3K
Manufacturer		Tejin Tenax	Toray Composite Materials America	Nippon Graphite Fibres (NGF)
Fibre precursor		PAN	PAN	Pitch
Tensile strength	[GPa]	4.4	5.49	3.53
Young's modulus	[GPa]	240	294	880
Ultimate strain	[%]	1.7	1.9	0.3
Filament diameter	[µm]	7	5	7

For the manufacture of the CFRP preform tubes, two different methods, well established in the industrial production of CFRP parts, were used (Figure 1). HT-fibre based tubes were manufactured via the prepreg wrapping method. Thereby, a cut sheet of 2D fibre fabrics, **pre**im**preg**nated with a defined amount of phenolic resin, was wrapped around a steel core. In order to fix and densify the prepreg laminate, a shrinkage tape was wrapped onto the prepreg laminate with defined tension. The resin was cured in a furnace at a maximum temperature of 220 °C for 2 hours in air. During the heating up, the tape was shrinking and pressure was applied on the laminate, which is necessary to obtain a sufficiently high fibre volume content and a low open porosity in the final CFRP tube.

For the IM and UHM fibres, wet filament winding was used to manufacture the CFRP preform tubes. Thereby, the fibre roving was impregnated with phenolic resin and wound on a rotating mandrel with a defined winding angel.

DOI: 10.13009/EUCASS2022-6114

Similar to the prepreg wrapping process, a shrinkage tape was applied on the final laminate. For the curing of the resin a similar process as for the prepreg wrapped tubes was used.
In this first approach, a winding angel of ± 54.7° relative to the tube axis was chosen, according to the net theory of composites [15], considering the 2:1 ratio of tangential and axial stresses in a thin walled, closed tube under inner pressure. In the fabric based, prepreg wrapped tubes the fibres were oriented in axial and circumferential direction (0°/90°), due the use of the 2D fabrics.

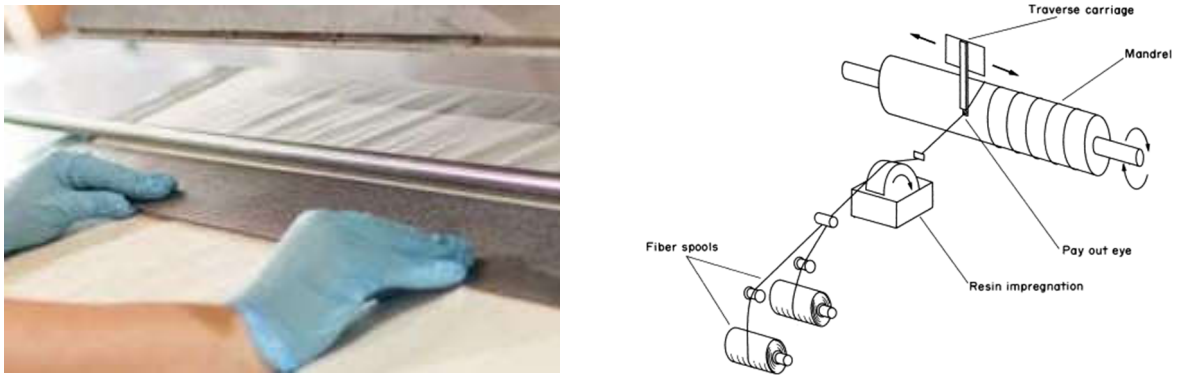

Figure 1 Manufacture of CFRP tubes via prepreg wrapping (left) and wet filament winding (right)

The fully automatized winding process ensures a high and reproducible quality of the resulting CFRP tubes. Due to the use of only one fibre roving, the manufacturing time for the winding up was quite long (8h) whereas the winding up of the prepreg is a matter of a few minutes. The main drawback of the prepreg wrapping is the use of costly prepregs, and the limited availability of prepregs with high performance fibres. Additionally, fibre orientation is restricted to 0°/90° or ± 45%, and therefore cannot be customized to the mechanical loads and stresses of the tube.

The CFRP preform tubes were pyrolyzed and siliconized using the LSI standard process as described before. In order to avoid delamination or distortion, graphite cores were used to stabilize the tubes during pyrolysis. After siliconization the tubes were cut to a length of 200 mm.

3. Sample Testing

Inner and outer diameter of the C/C and C/C-SiC tubes was measured with a calliper at eight positions on both ends of the tubes and a mean value was calculated. Fibre volume content was determined, considering the calculated area of the C/C tubes cross section and the calculated area of the of the carbon fibres, embedded in the cross section of the tubes. Open porosity and density of the C/C-SiC tubes were determined via Archimedes' method (DIN 51918). Material morphology and microstructure were investigated by SEM (Zeiss Gemini Ultra plus).
The stress/strain behaviour of the C/C-SiC tubes was tested under inner pressure load. Therefore, the C/C-SiC tubes were glued into steel adaptors and the pressure was applied using a manually operated hydraulic pump (Maximator M 72-01-HL), by pressing water into the tube. This led to a biaxial load of the tube. Ambient and inner pressure was measured using pressure sensors (Newport Omega PAA-33X-C-5; Range = 0 – 5 bar absolute; PA-33X/80794; Range = 0 – 300 bar absolute). For strain measurements, seven strain gauges (0° / 90°) were placed in the centre of the tube at equidistant positions on a circumferential and an axial line, in order to determine the strain in axial and tangential direction (Figure 2).

DOI: 10.13009/EUCASS2022-6114

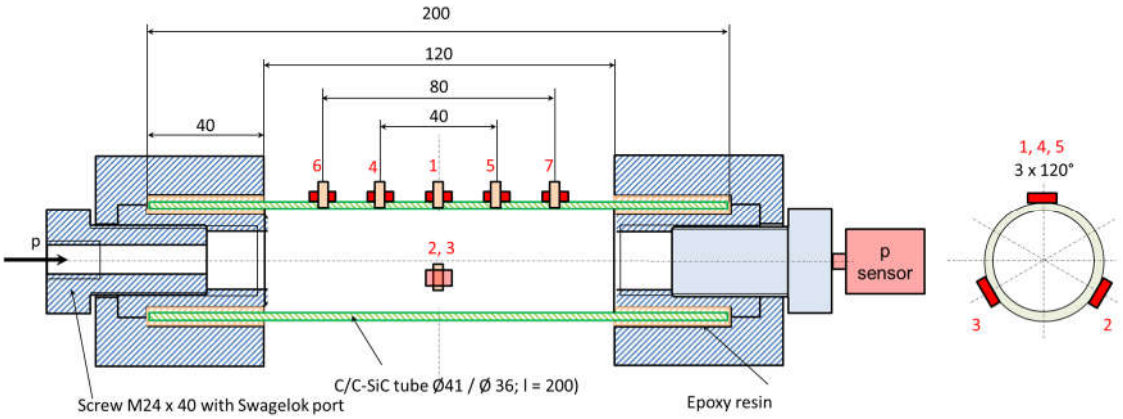

Figure 2 Test set up for inner pressure test of C/C-SiC tubes.

Tangential stress $\sigma_{tan.}$ (1) and axial stress $\sigma_{ax.}$ (2) in the tube wall was calculated using:

$$\sigma_{tan.} = p_i \cdot \frac{r_i^2}{r_o^2 - r_i^2} \cdot \left(\frac{r_o^2}{r_x^2} + 1\right) \quad (1)$$

$$\sigma_{ax.} = p_i \cdot \frac{r_i^2}{r_o^2 - r_i^2} \quad (2)$$

where p_i is the inner pressure, r_i and r_o is the inner and the outer radius of the tube and r_x is any desired radius of the tube wall [15]. Tangential fracture strength was calculated using the ultimate inner pressure $p_{i,u}$ obtained in the test as well as the ultimate stress $\sigma_{tan.,u}$ at the inner diameter of the tube ($r_x = r_i$). The differences in fibre contents of the tubes were considered by calculating a normalized stress $\sigma_{tan.,\,norm.}$ (3) using:

$$\sigma_{tan.,u,norm.} = \sigma_{tan.,u} \cdot \frac{\varphi_{f,nom.}}{\varphi_f} \quad (3)$$

where φ_f is the fibre volume content of the individual tube, and $\varphi_{f,\,nom.}$ = 55 % was chosen for the nominal fibre volume content.
Tangential elastic modulus E_{tan} was determined by the slope of the stress strain curve, using the stress calculated with (1) at the outer diameter ($r_x = r_o$) and the corresponding strain from the strain gauges, as well as using a nominal stress and the corresponding strain as upper limit. Thereby, the nominal stress $\sigma_{tan.nom.}$ = 51 MPa is the stress at the outer diameter of a reference tube with an outer and inner diameter of 41 and 36 mm, respectively, obtained at the nominal inner pressure of 60 bar, which is the maximum pressure required for the combustion chamber.

4. Results

The fibre volume content of the prepreg wrapped tubes (ϕ_f = 61.8 %) was 37 % higher compared to the tubes based on wet filament winding (Table 2), which was explained by the different fibre preforms and the pressure applied during laminating and curing. Open porosity was on a relatively low level for HT (e`= 4.6 %) and UHM (e´= 2.5 %) fibre based tube, whereas the IM-fibre based tube showed a high porosity of e`= 7.7 %, which was traced back to a high porosity in CFRP and an inconvenient curing process. The density of the HT and IM-fibre based tubes was 1.83 and 1.87 g/cm³, which is comparable to standard plate materials. UHM based tubes showed the highest density (ρ = 2.66 g/cm³), which was corresponding to previous experiments with plates [16]. The differences in density could be explained by the different microstructures and morphologies of the materials. Thereby, a high conversion rate of C fibres and C matrix generally lead to a high SiC content and finally to a high density of the C/C-SiC material. HT and IM fibre based tubes showed dense C/C blocks and only a small amount of SiC, created mainly at the boundary of the C/C blocks, whereas the microstructure of the UHM based tubes was characterized by an almost complete conversion

DOI: 10.13009/EUCASS2022-6114

of the C matrix and also of some single fibres to SiC, leading to a significantly higher SiC content and density compared to the HT and IM based tubes (Figure 3).

Table 2 Properties of tested CMC tubes.

Sample tube		HT 0°/90°	IM ± 54,7°	UHM ± 54,7°
Fiber type		HTA 40	T 800H	YS 90 A
Fiber preform		fabric	roving	roving
CFRP Manufacturing method		Prepreg wrapping	Wet filament winding	Wet filament winding
Fiber orientation	[°]	0°/90°	±54.7	±54.7
Inner diameter	[mm]	36.1	35.8	35.5
Outer diameter	[mm]	40.8	41.5	40.8
Fiber volume content in C/C	[Vol.-%]	61.8	45.1	44.8
Open porosity in C/C-SiC	[%]	4.6	7.7	2.5
Density in C/C-SiC	[g/cm³]	1.83	1.87	2.66
Ultimate pressure	[bar]	95.5	123.4	171.8
Standard deviation	[bar]	10.8	6.9	
Ultimate tangential stress	[MPa]	78.3	83.8	124.8
Standard deviation	[MPa]	9.59	0.81	
Fracture strength at nominal FVC	[MPa]	75.6	102.5	153.2
Ultimate tangential strain	[‰]	1.4	0.8	0.9
Standard deviation	[‰]	0.21	0.07	
Elastic modulus, tangentially	[GPa]	56.2	91.2	208.1
Standard deviation	[GPa]	4.18	6.96	
Ultimate axial stress at fracture	[MPa]	34.4	35.7	53.8
Standard deviation	[MPa]	4.3	0.7	
Ultimate axial strain at fracture	[‰]	0.42	0.65	1.02
Standard deviation	[‰]	0.01	0.13	
Elastic modulus, axially	[GPa]	81.4	58.6	90.7
Standard deviation	[GPa]	3.8	7.1	

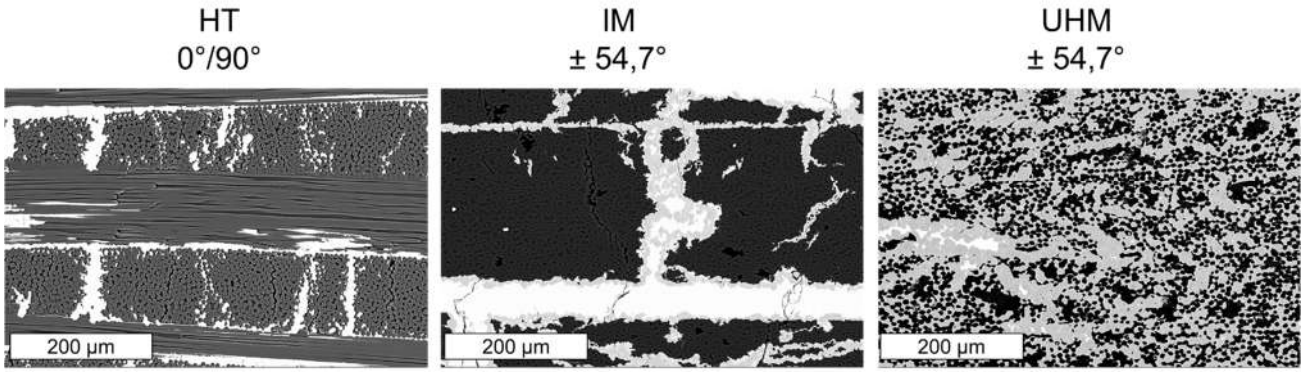

Figure 3 SEM images of the cross section of the different C/C-SiC tubes in tangential direction, showing C fibres and matrix (dark grey), SiC matrix (light grey), Si (white) and porosity (black).

DOI: 10.13009/EUCASS2022-6114

Fracture strength was highest for the UHM based tubes with an ultimate tangential stress of $\sigma_{tan.,u}$ = 125 MPa and a burst pressure of 172 bar, despite the fact that IM fibres offer a 55 % higher strength compared to the UHM fibres. Lowest strength was observed on HT based tubes, which was explained by the low fiber strength and the inconvenient fiber architecture. However, despite the unfavourable fibre orientation and the lower strength of the HT fibres, the fracture strength of the prepreg wrapped tubes was comparable to the filament wound IM tubes. Considering the different fibre contents of the tubes, the fracture strength of the IM tube was 36 % higher compared to the HT tube, and the fracture strength of the UHM tube was two times higher compared to the HT tube. Highest fracture strain was obtained with the fabric wrapped tubes ($\varepsilon_{tan.,u}$ = 1.39 ‰), which was 75 % higher compared to the IM tubes. The stress/strain behaviour of all tubes was nonlinear. However, the UHM tube showed an almost linear slope up to the nominal stress of 51 MPa.

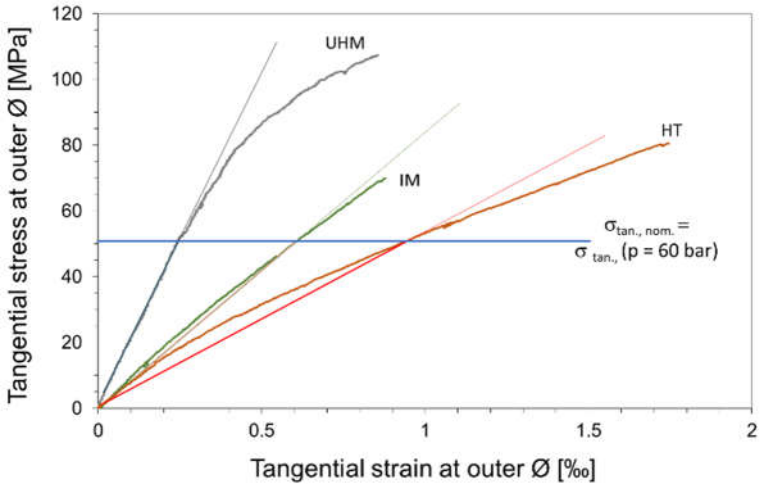

Figure 4 Representative stress / strain curves and slopes of the different C/C-SiC tubes, tested.

For the fabric wrapped tubes, the elastic modulus in tangential direction $E_{tan.,HT}$ = 56.2 GPa was comparable to the Young´s modulus usually obtained on flat sample plates. The tubes based on the IM fibres offered a 62 % higher modulus ($E_{tan.,IM}$ = 91.2 GPa), whereas the modulus of the UHM tubes was almost 4 times higher ($E_{tan.,UHM}$ = 208.1 GPa), compared to the HT tubes.
In axial direction the ultimate stress at fracture was only half of the tangential stress, as given by comparing (1) and (2). Due to the 0°/90° fibre orientation in the fabric wrapped tube, the axial strain at fracture ($\varepsilon_{ax.,u}$ = 0.42 ‰) was significantly lower compared to the corresponding tangential strain ($\varepsilon_{tan.,u}$ = 1.39 ‰). In contrast, for the filament wound IM and UHM tubes, the axial and tangential strain at fracture was on a comparable level, as expected from the fibre orientation in the tubes, indicating a well-designed tube laminate for the biaxial load scenario. Consequently, the resulting elastic modulus in axial direction was lower compared to the modulus in tangential direction. For the fabric-based tube with 0°/90° fibre orientation, a similar modulus in tangential and axial direction was expected and observed. The slightly higher value in axial direction was explained by the nonlinear stress strain behaviour, leading to a steeper slope at the lower stress level in axial direction, compared to the slope at higher stress level in tangential direction.

The failure behaviour of the tubes was characterized by a sudden fracture. The cracks were oriented perpendicular to the fibre orientation, indicating fibre dominant materials, as expected.

DOI: 10.13009/EUCASS2022-6114

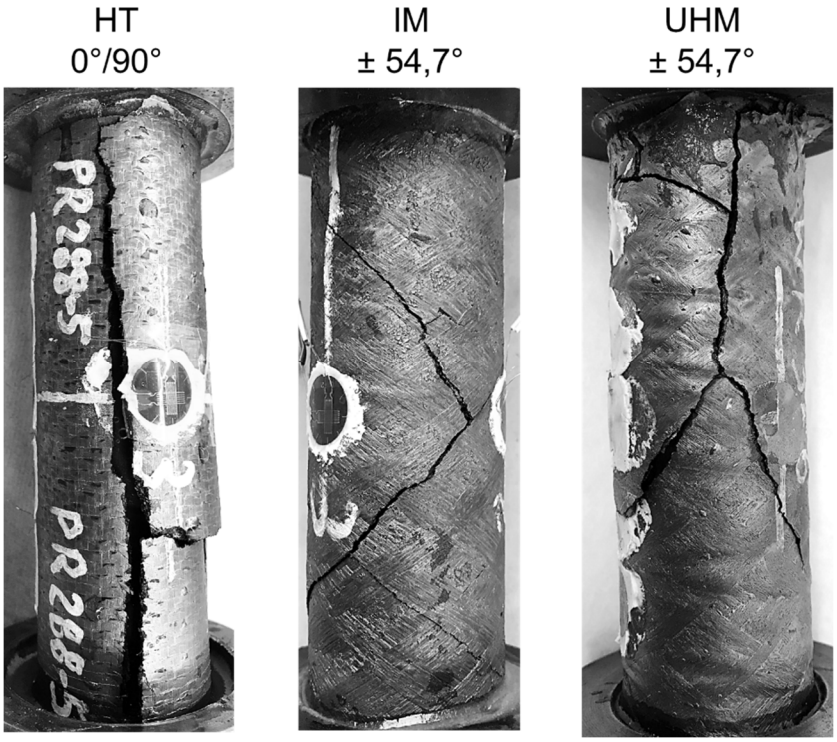

Figure 5 Failure behaviour of C/C-SiC tubes tested under inner pressure

5. Simulation

Accompanying the experimental tests, linear elastic FEM simulations of the HT 0°/90° fabric tube were performed in Ansys 2020R2 in order to demonstrate the viability of CMC-simulations and to validate the modelling and simulation method, as well as to determine possible stress peaks at the contact area between the pressure adaptors and the glued in test tube. Therefore, the geometry setup shown in Figure 6 was used. Whereas the isotropic parts (steel and resin) were modelled in Workbench, the anisotropic shaft was modelled as a layup structure in Ansys Composite PrePost (ACP).

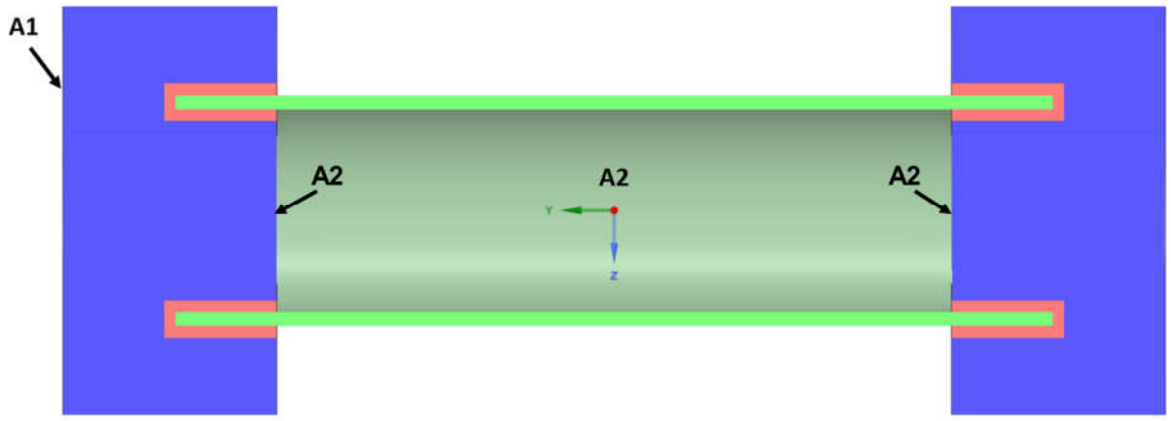

Figure 6 : Cross section of the geometry used for the simulations; blue: steel adaptors, green: C/C-SiC tube, red: epoxy resin adhesive

The pressure load of 60 bar was assumed as static and was applied to the inner surface of the tube and sealing caps (faces A2 in Figure 6). A fixed support was added on face A1. All touching faces were modelled as fixed contacts. Therefore, stresses were evaluated at least 3 elements away from the contacting nodes. The layup structure of the C/C-SiC tube consisted of 20 layers with a thickness of 0.1165 mm in order to achieve the desired wall thickness of 2.33 mm. A single layer was modelled, using the orthotropic properties shown in. The values for E_{11}, E_{22} and ν_{12} were

DOI: 10.13009/EUCASS2022-6114

derived via inverse laminate theory from the measured Youngs-Moduli from the tests. All other mechanical properties were taken from literature [17]. The layup angles were alternating between 0° and 90°. In ACP the classical laminate theory is used to compute the resulting laminate properties which are shown in Table 3. The axial and tangential Young's Moduli differ according to the measured test values (see Figure 4).

Table 3 Laminate properties

$E_{xx} = E_{axial}$	$E_{yy} = E_{tangential}$	G_{xy}	ν_{xy}
53.5	45.0	9.8	0.2

The strength values necessary for the calculation of the safety factors were taken from [17]. For the failure criterion, Tsai-Wu was chosen; the results can be seen in Figure 7. The minimum calculated Tsai-Wu factor was 2.06, which indicated no structural failure for the applied load of 60 bar. The result also indicated an even stress distribution over the whole axial length of the tube, which was desired for the tests, and determined the length of the test-tubes.

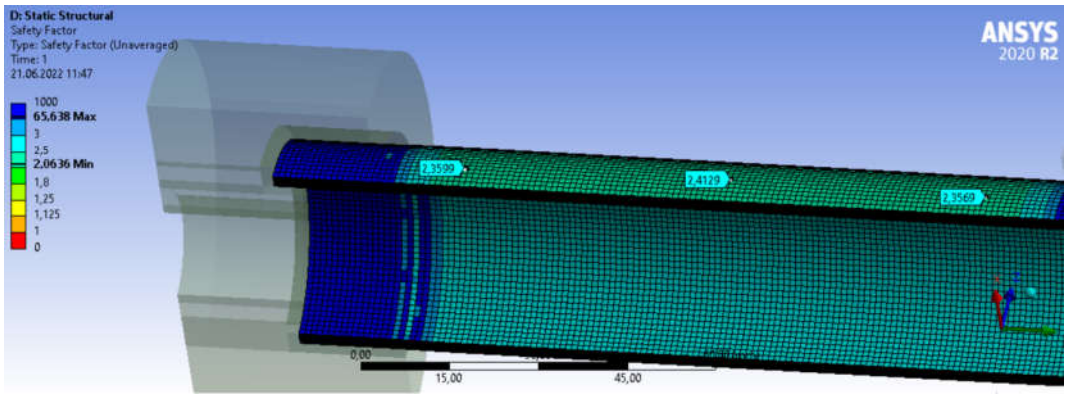

Figure 7 Calculated Tsai-Wu Factors of the tube

According to the simulation, structural failure would appear at 123,6 bar which is 11% higher than the maximum observed pressure of 110 bar. Since the strength values were taken from literature [17], and were determined on flat sample plates, this deviation was probably caused by differences between panel and tube material.

In Figure 8, the strain-results of the static, linear elastic simulation are summarized and compared to the measured strain values from the tests. Thereby, the strain values were taken from the outer surface of the tube at the same locations as the strain-gauges were located. Simulated strains in tangential direction ($\varepsilon_{tan.}$ = 0.93 ‰) were in good accordance with the strain data received from the strain gauges (0.94 ‰). In axial direction the simulated strain ($\varepsilon_{ax.}$ = 0.35 ‰) was also in good accordance, although a bit higher than the measured strain (0.31 ‰). The higher deviation in axial direction was traced back to the nonlinear stress/strain behaviour (Figure 4), leading to a deviating Young's Modulus, which was not captured by the linear-elastic simulation.

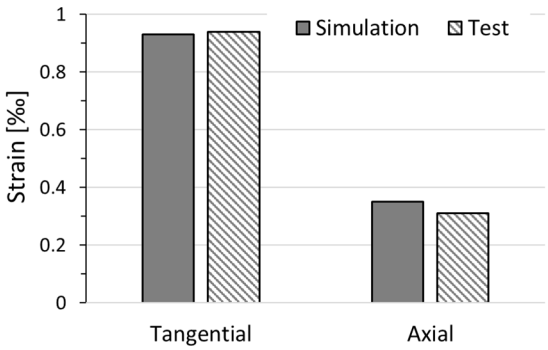

Figure 8 Comparison of simulated and measured strain in tangential and axial direction.

DOI: 10.13009/EUCASS2022-6114

6. Discussion

The mechanical properties of the C/C-SiC tubes were highly influenced by the carbon fibre type used. UHM fibre based tubes took advantage of the high tensile modulus of the fibres which lead to highest elastic modulus in tangential and axial direction of the tube. Compared to the IM tubes, which were manufactured in the same way as the UHM tube, elastic modulus was increased by a factor of 2.3 which was corresponding to the increase of the fibre modulus by a factor of three. However, the UHM tube also showed a 49 % higher fracture strength compared to the IM tube, despite the fact, that the fracture strength of the UHM fibre is 35 % lower. Additionally, the fracture strain of the IM tube was 11 % lower despite the 6 times higher fracture strain of the IM fibre, compared to the UHM fibre.
These effects were explained by the different failure mechanism of the UHM and IM fibres in the C/C-SiC composite material. The pitch-based fibres showed a quasiductile fracture behaviour, characterized by an internal fibre “pull-out”. Thereby, the fibre itself was split, leading to a large increase in fracture surface as described elsewhere [14]. This effect was explained by the highly turbostratic nature of the fibre structure and the characteristic large, sheet like crystals. In the C/C-SiC material, arising and propagating matrix cracks were deflected at the fibre / SiC matrix interface and inside the fibre itself, leading to high toughness. In contrast, PAN-based IM fibres showed a brittle fracture behaviour, without any energy dissipating pull-out effects in the fibre itself. Another reason for the low fracture strength and strain of the IM tubes was seen in the high open porosity of the IM tubes, which led to an insufficient embedding of the fibres in the composite and finally reduced the mechanical stability.
The HT tubes, cannot be directly compared to the tubes based on the high-performance fibres, due to the different manufacturing method and the use of a 2D fabric as fibre preform. However, fracture strength was comparable to the wet filament wound IM tubes, and the obtained fracture strain of 1.6 ‰ was highest for all tubes. This enables a robust design for mechanically highly loaded structural parts, due to an increased tolerance against uncertainties in load prediction, local overloads and damages. The high fracture strain was explained by the low conversion rate of the fibres to SiC, leading to a high content of load carrying C/C bundles and a low content of brittle SiC matrix in the C/C-SiC composite. Another advantage was the high fibre content above 60 vol.-%, which was possible by using fabric fibre preforms and the wrapping method. Thereby, high fracture strength can be obtained, generally leading to thin walled, lightweight structures.
Considering the fracture strength obtained by the inner pressure tests, a safety factor of 1.4, an inner diameter of 40 mm and a maximum pressure of 60 bar, the theoretically required minimum wall thicknesses would be 1.83 and 1.87 mm for HT and IM tubes, respectively, and 1.39 mm for UHM tubes. Taking into account the different densities of the material, the resulting minimum mass of UHM tubes would be 482 g/m, whereas the masses for the IM and HT tubes would be 524 g/m and 553 g/m, respectively.
From the economic point of view, prepreg wrapping offers a fast and cost-effective manufacturing method for the serial production of combustion chamber tubes. In order to overcome the restricted possibilities for adapting the fibre orientation to the load paths, biaxial nonwoven preforms with convenient fibre orientations would be a promising approach.

7. Internally cooled combustion chambers

In order to increase specific impulse, higher combustion temperatures are inevitably, and therefore, the development of regeneratively cooled CMC combustion chambers is in the focus. In a first feasibility study, an internally cooled C/C-SiC tube, based on an inner and outer liner tube and a corrugated core structure has been developed. Therefore, the prepreg wrapping method was used for the two tubes and the thin walled core (t = 0.3 mm) was manufactured using a newly designed mould. The individual parts were pyrolyzed separately, and the resulting C/C parts were assembled using tight fit tolerances between the core and the liner tubes, and finally siliconized (Figure 9).

DOI: 10.13009/EUCASS2022-6114

Figure 9 Demonstrator of an internally cooled C/C-SiC tube (Ø 40 mm / Ø 56 mm x 175 mm) based on liquid silicon infiltration (LSI) and in situ joining technology.

8. Conclusion

C/C-SiC tubes, manufactured via the cost-efficient liquid silicon infiltration process and two different, industrially common manufacturing methods for the CFRP preform, have been manufactured and tested successfully. Highest fracture strength and elastic modulus could be obtained with filament wound tubes based on UHM fibres, leading to thin walled and lightweight combustion chamber tubes. Since only a limited number of tubes could be tested in the frame of this work, additional tests are planned in order to confirm these results on a statistically reliable level.
Even more important, the thermal, abrasive and oxidative/corrosive properties of the materials will have a substantial influence on the material selection for future combustion chambers. These properties will be characterized in firing tests with integrated C/C-SiC combustion chamber liners. Thereby, significant advantages of the highly dense UHM fibre-based tubes are expected, due to their high SiC content, which should lead to high abrasive and oxidation resistance, as well as to a high thermal conductivity, which is very favourable for regeneratively cooled combustion chambers.

9. Outlook: Ceramic Combustion Chambers for Green Propellants

Worldwide the quest for green propellants is ongoing. A high performance, non-toxic, cheap and easy to handle green alternative to hydrazine is searched for. DLR is investigating several green propellants, among those are ADN based propellants □[18]□[19]□[20], hypergolic propellants based on hydrogen peroxide and ionic liquids □ ,[21]□ - [24], nitromethane-based propellants □[25], nitrous oxide/hydrocarbon mono- and bipropellants□[26]-□[31] as well as hydrogen peroxide as monopropellant □[32]. Across the globe, further alternatives as HAN-based propellants SHP-163 □[33] - □[35] or AF-M315E (ASCENT) □[36] - □[38] are investigated. Figure 10 shows the combustion temperature and corresponding specific impulse I_{sp} (4) for several green propellants and hydrazine. The specific impulse I_{sp} is proportional to the square root of the combustion temperature T_c divided by the molecular weight M of the exhaust gases:

$$I_{sp} \sim \sqrt{\frac{T_C}{M}} \tag{4}$$

This means, that a higher specific impulse is directly connected to a higher combustion temperature. If new propellant and propellant combinations with a higher Isp than hydrazine are developed, the combustion temperature of these propellants rises accordingly. This is visible in Figure 10, the new propellant formulations come along with higher combustion temperatures than hydrazine. As a consequence, for these green alternatives, new combustion chamber materials or cooling methods are needed. Here, CMC chamber materials offer the possibility of lightweight thrusters with a higher allowed operational temperature than conventional refractory metals. In general, two applications for ceramic materials are possible: Uncooled ceramic structures as replacement for conventional high

DOI: 10.13009/EUCASS2022-6114

temperature materials or cooled structures for regenerative cooled thrusters. Both applications will be investigated in the successor project of DLR's "Future Fuels" project [29], [39], which is now called "NeoFuels".

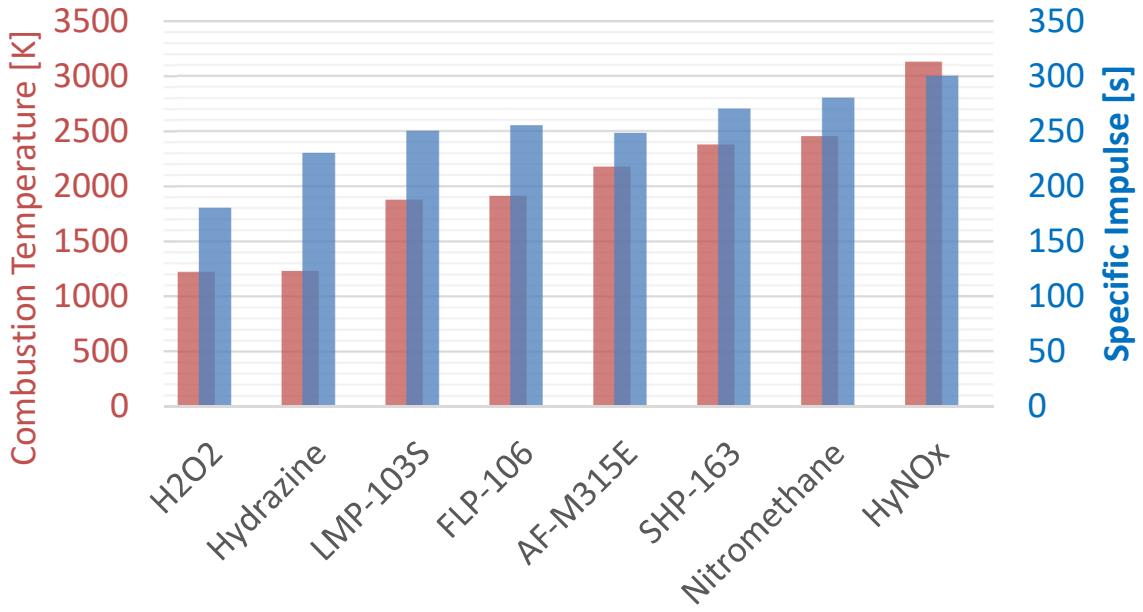

Figure 10 Combustion temperature and specific Impulse (Isp) of several green propellants and hydrazine [32], [33], [35], [36], [40] - [46].

References

[1] Ciezki, H.K. and Naumann, K.W., (2016) Some Aspects on Safety and Environmental Impact of the German Green Gel Propulsion Technology, Propel., Explos., Pyrotech., 41(3), pp. 539–547

[2] Hodge, K., Crofoot, T., and Nelson, S., (1999) Gelled Propellants for Tactical Missile Applications, in 35th Joint Propulsion Conf. and Exhibit.

[3] Natan, B., & Hasan, D. (2019). ADVANCES IN GEL PROPULSION. International Journal of Energetic Materials and Chemical Propulsion, 18(4).

[4] Kurilov, M., Kirchberger, C. U., Freudenmann, D., Stiefel, A. D., & Ciezki, H. K. (2018). A Method for Screening and Identification of Green Hypergolic Bipropellants. International Journal of Energetic Materials and Chemical Propulsion, 17(3).

[5] Kurilov, M., Kirchberger, C., Freudenmann, D., Ricker, S., Ciezki, H., & Schlechtriem, S. (2021). Investigation of novel metallized monopropellants.

[6] Ricker, S., Kurilov, M., Freudenmann, D., Kirchberger, C., Hertel, T., Ciezki, H., & Schlechtriem, S. (2019). Novel gelled fuels containing nanoparticles as hypergolic bipropellants with HTP. In Proceedings of the 8th European Conference for Aeronautics and Space Sciences.

[7] Madlener, K., & Ciezki, H. K. (2012). Estimation of flow properties of gelled fuels with regard to propulsion systems. Journal of Propulsion and Power, 28(1), 113-121.

[8] Stiefel, A. (2019). Die Strömungseigenschaften von Gelen am Beispiel einer injektorähnlichen Geometrie (Doctoral dissertation, Universität Stuttgart).

[9] Krenkel, W. (2000). Entwicklung eines kostengünstigen Verfahrens zur Herstellung von Bauteilen aus keramischen Verbundwerkstoffen, Doctoral Thesis, Unversity of Stuttgart, DLR Forschungsbericht 2000-4.

[10] Koehler, R. J. (2001) Manuscript of the presentation at the shareholders meeting of the SGL Carbon Group 2001, Germany.

[11] Biffi, R., Zäch, B. (2002) Schindler 700 – the Journey to the Top, Schindler Elevators, http://www.schindler.com/com/internet/en/media/press-releases-english/press-releases-2006-2000/schindler-700-the-journey-to-the-top.html.

[12] B. Heidenreich, B., Zuber, C., Toro, S., Nardi, M. (2013) C/C-SIC Friction pads for an aircraft propeller brake, DGM Verbundwerkstoffe Karlsruhe 2013, Ed. A. Wanner/K.A. Weidenmann, ISBN 978-3-00-04230919, 19. Symposium Verbundwerkstoffe und Werkstoffverbunde, 03.- 05.07.2013, Karlsruhe

[13] Verberne, O. (2006) Jet Vane Production Facilities Operational, Nammo bulletin 2006, www.nammo.com.

[14] Reimer, T., Petkov, I., Koch, D., Frieß, M., Dellin, C. (2014) Fabrication and Characterization of C/C-SiC Material made with Pitch-Based Carbon Fibres, MS&T 2014 Ceramic Transactions.
[15] Altenbach, H. (2014) Holzmann/Meyer/Schumpich Technische Mechanik Festigkeitslehre, Springer Vieweg Wiesbaden, Ed. 11, https://doi.org/10.1007/978-3-658-06041-1.
[16] Schneck, T. K., Brück, B., Schulz, M., Spörl, J. M., Hermanutz, F., Clauß, B., Mueller, W. M., Heidenreich, B., Koch, D., Horn, S., Buchmeiser, M. R. (2019) "Carbon Fibre Surface Modification for Tailored Fibre-Matrix Adhesion in the Manufacture of C/C-SiC Composites," Composites, Part A, 120, 64-72.
[17] Yuan, S. (2017) Characterization and modeling of the mechanical properties of wound oxide ceramic composites. DLR-Forschungsbericht. DLR-FB-2017-30. Dissertation. Karlsruher Institut für Technologie (KIT). 130 S. doi: 10.5445/IR/1000070478.
[18] M. Wilhelm et al., "The RHEFORM Project - Developments for ADN-Based Liquid Monopropellant Thrusters," in 53rd AIAA/SAE/ASEE Joint Propulsion Conference, 10-12 July 2017, Atlanta, GA, USA, 2017.
[19] M. Negri et al., "New technologies for ammonium dinitramide based monopropellant thrusters – The project RHEFORM," Acta Astronautica, vol. 143, no. 1, pp. 105–117, 2018, doi: 10.1016/j.actaastro.2017.11.016.
[20] C. Hendrich et al., "Ignition of ADN-based Monopropellants - Results of the European Project RHEFORM," in 68th International Astronautical Congress 2017, 25-29. September 2017, Adelaide, Australia. Accessed: May 31 2022. [Online]. Available: https://elib.dlr.de/118042/1/Hendrich_2017_IAC.pdf
[21] M. Negri and F. Lauck, "Hot Firing Tests of a Novel Green Hypergolic Propellant in a Thruster," Journal of Propulsion and Power, pp. 1–11, 2022, doi: 10.2514/1.B38413.
[22] F. Lauck, J. Witte, M. Negri, D. Freudenmann, and S. Schlechtriem, "Design and first results of an injector test setup for green hypergolic propellants," in AIAA Propulsion and Energy 2019 Forum, p. 163.
[23] F. Lauck, M. Negri, D. Freudenmann, and S. Schlechtriem, "Selection of ionic liquids and characterization of hypergolicy with hydrogen peroxide," Int J Energetic Materials Chem Prop, vol. 19, no. 1, pp. 25–37, 2020, doi: 10.1615/IntJEnergeticMaterialsChemProp.2019028004.
[24] F. Lauck, M. Negri, D. Freudenmann, and S. Schlechtriem, "Study on hypergolic ignition of ionic liquid solutions," in 8th European Conference for Aeronautics and Space Sciences (EUCASS), 1.-4. July 2019, Madrid, Spain.
[25] M. Kurilov, L. Werling, M. Negri, C. Kirchberger, and S. Schlechtriem, "Impact Sensitiveness of nitromethane-based green propellant precursors mixtures," in 8th Space Propulsion Conference 2022, 09-13. May 2022, Estoril, Portugal.
[26] L. K. Werling et al., "Nitrous Oxide Fuels Blends: Research on Premixed Monopropellants at the German Aerospace Center (DLR) since 2014," in AIAA Propulsion and Energy Forum and Exposition, 2020. AIAA Propulsion and Energy Forum 24.-26.08.2020, 24.-26.08.2020.
[27] L. Werling et al., "High Performance Propellant Development - Overview of Development Activities Regarding Premixed, Green N2O/C2H6 Monopropellants," in 8th Space Propulsion Conference 2022, 09-13. May 2022, Estoril, Portugal.
[28] Lukas Werling, "Entwicklung und Erprobung von Flammensperren für einen vorgemischten, grünen Raketentreibstoff aus Lachgas (N2O) und Ethen (C2H4): DLR-Forschungsbericht. DLR-FB-2020-39, 330 S," Dissertation, Institut für Raumfahrtsysteme, University of Stuttgart, Stuttgart, 2020.
[29] T. Pregger et al., "Future Fuels—Analyses of the Future Prospects of Renewable Synthetic Fuels," Energies, vol. 13, no. 1, p. 138, 2020, doi: 10.3390/en13010138.
[30] L. Werling and P. Bätz, "Parameters Influencing the Characteristic Exhaust Velocity of a Nitrous Oxide/Ethene Green Propellant," Journal of Propulsion and Power, vol. 38, no. 2, pp. 254–266, 2022, doi: 10.2514/1.B38349.
[31] L. Werling and T. Hörger, "Experimental analysis of the heat fluxes during combustion of a N 2 O/C 2 H 4 premixed green propellant in a research rocket combustor," Acta Astronautica, vol. 189, pp. 437–451, 2021, doi: 10.1016/j.actaastro.2021.07.011.
[32] F. Lauck et al., "Test bench preparation and hot firing tests of a 1N hydrogen peroxide monpropellant thruster," in Space Propulsion Conference 14.-18.05.2018, Sevilla, Spain.
[33] T. Katsumi and K. Hori, "Successful development of HAN based green propellant," Energetic Materials Frontiers, vol. 2, no. 3, pp. 228–237, 2021, doi: 10.1016/j.enmf.2021.09.002.
[34] K. Hori, "Lessons Learned in the Thruster Tests of HAN," in Springer Aerospace Technology, Chemical Rocket Propulsion: A Comprehensive Survey of Energetic Materials, Cham, s.l.: Springer International Publishing, 2017, pp. 801–818.
[35] K. Hori, T. Katsumi, S. Sawai, N. Azuma, K. Hatai, and J. Nakatsuka, "HAN-Based Green Propellant, SHP163 – Its R&D and Test in Space," Prop., Explos., Pyrotech., vol. 44, no. 9, pp. 1080–1083, 2019, doi: 10.1002/prep.201900237.
[36] R. L. Sackheim and R. K. Masse, "Green Propulsion Advancement: Challenging the Maturity of Monopropellant Hydrazine," Journal of Propulsion and Power, vol. 30, no. 2, pp. 265–276, 2014, doi: 10.2514/1.b35086.

DOI: 10.13009/EUCASS2022-6114

[37] R. K. Masse, R. Spores, and M. Allen, “AF-M315E Advanced Green Propulsion – GPIM and Beyond,” in AIAA Propulsion and Energy 2020 Forum, VIRTUAL EVENT, 08242020.
[38] R. Masse, M. Allen, R. Spores, and E. A. Driscoll, “AF-M315E Propulsion System Advances and Improvements,” in 52nd AIAA/SAE/ASME Joint Propulsion Conference, 25.-27. July 2017, Salt Lake City, Utah, USA, 2017.
[39] H. K. Ciezki et al., “Advanced Propellants for Space Propulsion - A Task within the DLR Interdisciplinary Project "Future Fuels",” in 8th European Conference for Aeronautics and Space Sciences (EUCASS), 1.-4. July 2019, Madrid, Spain. Accessed: Sep. 3 2019. [Online]. Available: http://www.eucass2019.eu/
[40] A. Sarritzu, L. Blondel-Canepari, R. Gelain, P. Hendrick, and A. Pasini, “Trade-off study of green technologies for upper stage applications,” in 8th Space Propulsion Conference 2022, 09-13. May 2022, Estoril, Portugal.
[41] S. Gordon and B. McBride, Computer Program for Calculation of Complex Chemical Equilibrium Compositions and Applications: NASA Reference Publication 1311. I. Analysis, 1996.
[42] M. Persson, K. Anflo, and P. Friedhoff, “Flight Heritage of Ammonium Dinitramide (ADN) Based High Performance Green Propulsion (HPGP) Systems,” Prop., Explos., Pyrotech., vol. 44, no. 9, pp. 1073–1079, 2019, doi: 10.1002/prep.201900248.
[43] M. Persson, K. Anflo, A. Dinardi, and J. Bahu, “A Family of Thrusters for ADN-Based Monopropellant LMP-103S,” in 48th AIAA/ASME/SAE/ASEE Joint Propulsion Conference & Exhibit, Atlanta, Georgia.
[44] A. S. Gohardani et al., “Green space propulsion: Opportunities and prospects,” Progress in Aerospace Sciences, vol. 71, no. 1, pp. 128–149, 2014, doi: 10.1016/j.paerosci.2014.08.001.
[45] A. E. S. Nosseir, A. Cervone, and A. Pasini, “Review of State-of-the-Art Green Monopropellants: For Propulsion Systems Analysts and Designers,” Aerospace, vol. 8, no. 1, p. 20, 2021, doi: 10.3390/aerospace8010020.
[46] L. Werling, M. Hassler, F. Lauck, H. K. Ciezki, and S. Schlechtriem, “Experimental Performance Analysis (c* & c* Efficiency) of a Premixed Green Propellant consisting of N2O and C2H4 ,” in 53rd AIAA/SAE/ASEE Joint Propulsion Conference, 10-12 July 2017, Atlanta, GA, USA, 2017.